YingLong-I: A Hybrid Aerial Underwater Vehicle Using Integrated Coaxial Counter-Rotating Propulsion

Le Huang, *Student Member, IEEE*, Qirong Lei, *Student Member, IEEE*, Shuxiang Guo, *Fellow, IEEE*, Chunying Li, *Member, IEEE*, Guoheng Ma, Haotian Sun, *Student Member, IEEE*, and Shuaixin Peng

***Abstract*—A compact and lightweight hybrid aerial underwater vehicle(HAUV) named YingLong-I is proposed in this letter. The system primarily consists of an integrated coaxial counter-rotating propulsion module, a rudder-based air-water compatible attitude control module, and an attitude switching module, with a compact size of 292 × 292 × 405 mm and a total weight of 2.5 kg. Compared to seperate air-water propulsion modules, the integrated coaxial counter-rotating propulsion module significantly reduces structural volume and weight. Simultaneously, consistent attitude regulation across both aerial and underwater environments is ensured by the unified rudder-based attitude control module. A payload-to-weight ratio of 0.46 (maximum payload: 1.2 kg) is demonstrated by YingLong-I, surpassing quadrotor HAUVs, where ratios are typically below 0.3. The capabilities of YingLong-I, including cross-domain transition, stable aerial flight, underwater navigation, depth-keeping, and vertical takeoff/landing, were verified through field experiments.**

***Index Terms*—Field robots, mechanism design, hybrid aerial underwater vehicle(HAUV), integrated propulsion.**

I. Introduction

HAUVs are emerging as a versatile vehicle class capable of aerial, underwater, and seamless air-water transition operations. Their unique advantages lie in underwater navigation for stealth and energy-efficient long-duration missions [1], [2], [3], alongside aerial flight for high-speed transit. These capabilities make HAUVs highly promising for applications ranging from air-sea integrated maintenance to environmental monitoring as shown in Fig. 1.

Current HAUV designs (fixed-wing, multi-rotor, hybrid fixed-wing/multi-rotor, and bio-inspired flapping-wing) face two core challenges: (1) balancing compactness against payload capacity and energy efficiency; (2) developing lightweight integrated propulsion and attitude control modules for dual media.

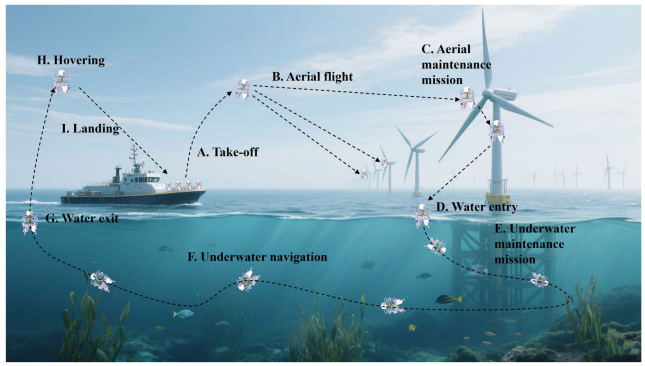

Fig. 1. YingLong-I multi-domain application illustration.

Fixed-wing HAUVs are efficient but large and less flexible [4]. While multi-rotor ones provide structural simplicity and vertical takeoff and landing (VTOL)/hovering capabilities, their large rotor spacing compromises compactness, significantly increasing hydrodynamic drag [5]. These designs also typically exhibit limited payload capacity and high energy consumption. Hybrid designs merge aerial efficiency with VTOL capability at the cost of increased volume and complexity [6]. Most implementations employ separate propulsion modules [7], [8], which increase system mass and volume, reducing payload capacity and increasing power consumption.

To address these challenges, this letter introduces YingLong-I, featuring: an integrated coaxial counter-rotating propulsion module for reduced bulk, enhanced efficiency and payload capacity; and a cross-media rudder-based attitude control module for unified control, drag and volume reduction.

II. Related Works

Fixed-wing HAUVs, such as Dipper [4] and Longbow II [7], use wing folding mechanisms to reduce size and hydrodynamic drag during water entry. However, their folded dimensions (Dipper: 1.16 × 0.4 m; Longbow II: 1.95 × 0.67 m) remain large, restricting deployment flexibility. Moreover, their payload efficiency is low; for instance, Longbow II can only carry 1 kg of payload at a total mass of 13.3 kg, yielding a 7.5% payload ratio.

Received 25 March 2025; accepted 21 July 2025. Date of publication 1 August 2025; date of current version 7 August 2025. This article was recommended for publication by Associate Editor S. Hamaza and Editor G. Loianno upon evaluation of the reviewers' comments. This work was supported in part by the GuangDong Basic and Applied Basic Research Foundation General Program under Grant 2025A1515011007, in part by Shenzhen Science and Technology Program under Grant RCBS20231211090725048, and in part by the High level of special funds from Southern University of Science and Technology under Grant G03034K003. *(Corresponding authors: Shuxiang Guo; Chunying Li.)*

The authors are with the Department of Electronic and Electrical Engineering, Southern University of Science and Technology, Shenzhen 518055, China (e-mail: huangl2023@mail.sustech.edu.cn; guo.shuxiang@sustech.edu.cn; licy@sustech.edu.cn).

This article has supplementary downloadable material available at https://doi.org/10.1109/LRA.2025.3595049, provided by the authors.

Digital Object Identifier 10.1109/LRA.2025.3595049

Puppala et al. proposed Acutus, a transformable multi-rotor HAUV with propeller-retraction into streamlined shells [5]. Nezha-F uses foldable arms with a piston variable buoyancy system [9]. While these folding strategies enhance compactness and reduce drag, they add mechanical weight/volume and reduce reliability. Maia et al. designed an octo-quadcopter HAUV with coaxial propellers for enhanced cross-domain transitions [10], but its underwater propulsion relies on aerial propellers, compromising hydrodynamic efficiency. Bi et al. developed the bone-shaped Nezha-B HAUV [8], using a double-layer quadrotor to minimize size and weight (0.4 m $\times$ 0.124 m, 900 g), though at the cost of payload capacity and roll control performance.

Compared with multi-rotor HAUVs, coaxial counter-rotating HAUVs offer distinct advantages. Their coaxial design enables larger rotor area in similar dimensions, directly improving payload capacity and flight efficiency [11]. Notably, they replace the energy-intensive differential motor speed control of multi-rotors with swashplates or rudders for pitch/roll regulation, significantly reducing maneuver power consumption [12]. The streamlined coaxial structure also enhances compactness and maneuverability, while dual-layer propellers facilitate smoother air-water transitions [10].

However, research on coaxial counter-rotating HAUVs remains limited. Zhang et al. proposed a foldable coaxial rotor system and developed dynamic models for cross-domain operation [12], but this work relied solely on simulations without physical prototype validation. Gao et al. designed a coaxial HAUV with foldable blades, a tilting platform, and a center of gravity (CoG) movement-based attitude switch system [13]. While their prototype demonstrated strong lift performance (40 kgf lift, 25-min aerial flight with a self-weight of 13.3 kg), separate propulsion modules (4.4 kg aerial, 1.2 kg underwater) increased system mass. Cross-domain transition efficiency was suboptimal (25 s mode switching, 60 s water-to-air), and key speed metrics were unreported. Wang et al.'s "ABDragon" achieved a 2 s water-air transition [14] but only allowed vertical underwater movement, lacking horizontal navigation capability.

HAUV propulsion modules are categorized as seperate or integrated air-water types. Seperate configurations [7], [13] allow medium-specific optimization but increase weight and size, reducing payload capacity. For integrated propulsion, Alzu'bi et al. pioneered the simplest approach of using aerial propellers for both media, requiring low speeds ($\leq$180 rpm) to avoid underwater cavitation [15]. This approach highlights a core challenge: propellers optimized for air typically underperform underwater, as noted by Yao et al. [16]. Tan et al. later introduced a 12 g dual-speed transmission structure with planetary gearsets, enabling shifts between direct-drive aerial and reduced-speed underwater modes [17], but this design incurred 18% aerial and 24% underwater efficiency losses due to transmission friction. Liu et al. simplified the design by eliminating a gearset [18], yet both systems shared a critical flaw: air-optimized propellers performed poorly underwater.

YingLong-I advances beyond prior work by: (1) The integrated coaxial counter-rotating propulsion, using reversible motors and passive one-way bearings, eliminates gearsets, simplifies mechanical structure, reduces weight and volume, minimizes energy loss, and enables aerial-underwater propeller switching for dual-medium efficiency. (2) The unified rudder-based control module replaces tilt-plate mechanisms, enabling cross-media usability and reducing vehicle size and drag. (3) Adopting a coaxial dual-propeller configuration with an adapted frame structure enhances payload capacity and flight efficiency. The frame design also serves as a protective structure, safeguarding components and the environment during failures.

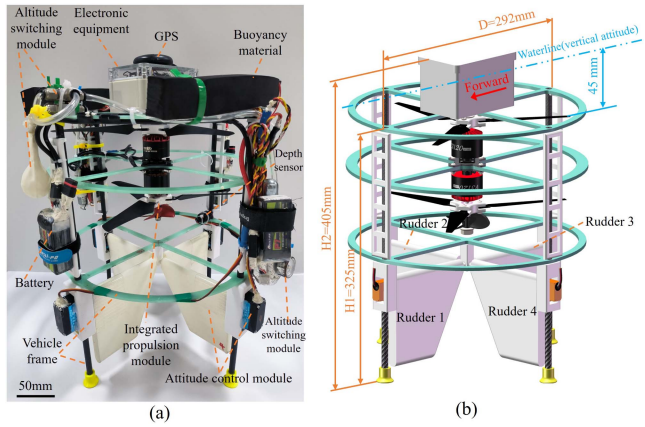

Fig. 2. YingLong-I prototype overview. (a) Prototype photograph with key components. (b) 3D model with dimensions.

Comparative performance is quantified in Table I, with detailed experimental validation discussed in Section V.

III. Structure and Mechatronics

A. Configuration Overview

The YingLong-I prototype is primarily composed of several key parts. As shown in Fig. 2(a), these include a frame, an integrated coaxial counter-rotating propulsion module, an air-water compatible attitude control module, an attitude-switching module, and electronic equipment. YingLong-I has dimensions of 292 $\times$ 292 $\times$ 405 mm ($L \times W \times H$) (Fig. 2(b)). As Table II shows, battery takes up the largest share in the component weight distribution(28%).

B. Integrated Coaxial Counter-Rotating Propulsion Module

Designing an integrated propulsion module requires addressing three key requirements: high-efficiency thrust generation in both air and water, minimized size/weight to reduce flight burden and water drag, and simplified structure for reliability.

To fulfill these requirements, we developed a novel integrated propulsion unit (Fig. 3(a)) featuring a one-way bearing. It uses dedicated aerial/underwater propellers directly driven for maximum dual-medium efficiency. As shown in Fig. 3(b), rotation direction controls mode via the bearing: counterclockwise engages the aerial propeller, while clockwise disengages it, activating the underwater screw. Though the underwater screw rotates during flight (gray dashed arrow in Fig. 3(b)), its small size (1/5th the diameter of the aerial propeller) and underwater-optimized design minimize its aerial thrust contribution(less than 1 N by experiment).

YingLong-I's entire integrated coaxial counter-rotating propulsion module contains an upper aerial independent

TABLE I
COMPARISON OF TECHNICAL PARAMETERS FOR EXISTING HAUVS

Parameter	Longbow-II [7]	Nezha-B [8]	TJ-FlyingFish [18]	TDAV [13]	Our Prototype
Type	Fixed-wing	Multi-rotor	Multi-rotor	Coaxial	Coaxial
Dimensions (L×W×H, m)	1.95×2.535 × –	0.412×0.102×0.101	0.438×0.438×0.500	1.215×0.166×0.166	0.292×0.292×0.405
Weight (kg)	13.3	0.9	1.63	16.3	2.5
Payload capacity (kg)	0.995	–	–	–	1.173
Propulsion type	Separated	Separated	Integrated	Separated	Integrated
Propulsion weight (kg)	Air: – Underwater: 0.398	Air: 0.16 Underwater: 0.03	0.488	Air: 4.4 Underwater: 1.2	0.392
Battery capacity	6400 mAh (12S LiPo)	2200 mAh (4S LiPo)	2200 mAh (4S LiPo)	16000 mAh (12S LiPo)	2200 mAh (12S LiPo)
Max. flight speed (m/s)	44.7	5.0	–	–	5.4
Flight endurance (min)	10–15	–	6.0	25.0	7.5
Max. submerged speed (m/s)	1.23	1.67	0.30	–	1.8
Submerged endurance (min)	57–69	–	40.0	55.0	50.0
Water-exit time (s)	13–15	2.0	–	60.0	3.2
Water-entry time (s)	0.6–1.6	–	–	155.0	1.0

TABLE II
WEIGHT AND PROPORTION OF COMPONENTS

Component Name	Weight	Proportion
Battery	$720g$	28%
Vehicle Frame	$500g$	20%
Air-water integrated propulsion system	$392g$	15%
Attitude control system	$312g$	13%
Attitude switch system	$298g$	12%
Electronics	$176g$	7%
Electronics compartment	$90g$	3%
Others(cables, fasteners etc.)	$57g$	2%

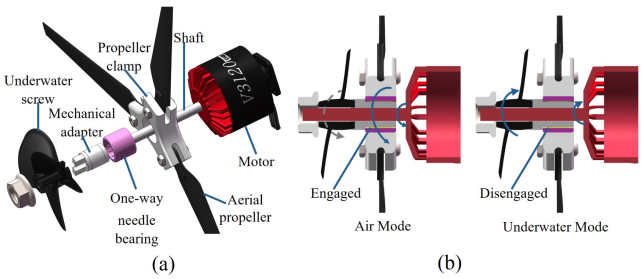

Fig. 3. Yinglong-I integrated coaxial counter-rotating propulsion module design. (a) Exploded diagram of integrated air-water propulsion unit. (b) Different propulsion modes via motor rotation direction.

propulsion unit and a lower air-water integrated propulsion unit(Fig. 2(b)). During flight, the upper and lower motors contra-rotate aerial propellers to generate coaxial thrust. For underwater operation, only the lower motor activates in clockwise rotation, driving the underwater screw for submerged propulsion.

C. Air-Water Compatible Attitude Control Module

As shown in Fig. 2(a), the attitude control module consists of four rudder-servo pairs. This design enables consistent operation in both air and water: rudders generate control torques by deflecting within the fluid flow of the propellers. In aerial mode, coordinated rudder pairs (groups 1&3 and 2&4) control roll and pitch by interacting with the aerial propeller airflow. Yaw control is achieved through differential propeller speeds. In underwater mode, individual rudder deflections within the underwater propeller's water flow control roll, pitch and yaw.

To evaluate the rudder-based attitude control effectiveness and calculate rudder dimensions, a theoretical analysis is performed. It assumes hovering or low-speed flight and small rudder deflections ($<15°$), and quantifies rudder torques about the vehicle's CoG and the required servo torque.

The propeller thrust $T(N)$ is computed using:

$$T = C_T \rho n^2 D^4 \tag{1}$$

where C_T is the thrust coefficient, $\rho(\text{kg/m}^3)$ the fluid density, $n(rps)$ the rotational speed, and $D(m)$ the propeller diameter.

The propeller-induced velocity V is derived using the following equations. v_i denotes the induced velocity of a single propeller, while v_{i1} and v_{i2} represent the induced velocities of the upper and lower rotors in the coaxial configuration, respectively. Accounting for downwash interference from the upper rotor, the lower rotor's induced velocity is corrected by a factor $k = 0.75$:

$$T = 2\rho A v_i^2, \quad A = \frac{\pi D^2}{4} \tag{2}$$

$$v_i = nD\sqrt{\frac{2C_T}{\pi}} \tag{3}$$

$$v_{i2} = k v_{i1} \tag{4}$$

$$V = (1+k)v_{i1} = (1+k)nD\sqrt{\frac{2C_T}{\pi}} \tag{5}$$

Using the induced airflow velocity V, the aerodynamic forces and moments exerted on the rudders are calculated:

$$F_N = C_N q S, \quad C_N \approx 2\pi\beta, \quad q = \frac{1}{2}\rho V^2 \tag{6}$$

$$d = \frac{l}{2} + h\cos\beta \tag{7}$$

$$\tau_{att} = 2F_N \cdot d = 4\beta\rho C_T (1+k)^2 n^2 D^2 S\left(\frac{l}{2} + h\cos\beta\right) \tag{8}$$

$$\tau_{rot} = F_N \cdot \frac{l}{2} = \beta\rho C_T (1+k)^2 n^2 D^2 S l \tag{9}$$

Here, F_N is the normal force, τ_{att} the attitude control torque, and τ_{rot} the servo rotation torque. The normal force coefficient

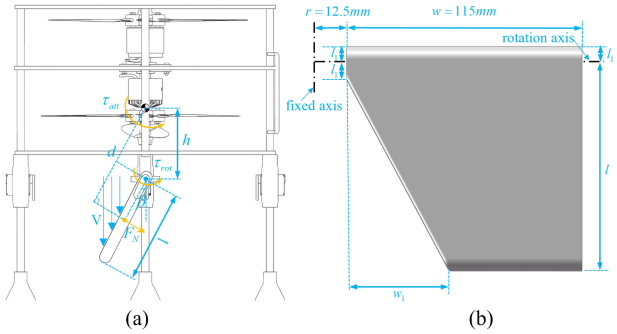

Fig. 4. (a) Attitude control mechanism. (b) Rudder shape design and parameters.

C_N(approximated using fixed-wing lift theories) depends on rudder deflection angle β. q denotes downwash dynamic pressure, and S is the rudder area. Geometric parameters in Fig. 4 are: moment arm d (from rudder center to CoG), rudder length l, and distance h (vertical from CoG to rudder axis).

The effectiveness of rudder control is analyzed by comparing the generated torques to the primary opposing torques: inertial torque and gravitational restoring torque. Aerodynamic damping is neglected for this analysis.

Newton's second law gives the inertial torque for pitch/roll angular acceleration:

$$\tau_{inertia} = I \cdot \alpha, \tag{10}$$

where I is the HAUV's rotational inertia about the axis and α is the angular acceleration.

For YingLong-I, the CoG positioned below the center of lift (CoL) generates a gravitational restoring torque during pitch/roll tilting:

$$\tau_{gravity} = G \cdot d_{lg} \cdot \sin(\theta), \tag{11}$$

where G is the vehicle weight, d_{lg} the vertical distance between CoL and CoG, and θ the body tilt angle.

Adequate control authority requires:

$$\tau_{att} > \tau_{\text{inertia}} + \tau_{\text{gravity}} \tag{12}$$

The basic rudder shape design and parameters are shown in Fig. 4(b). Width w is determined by the installation space. Length l_1 and width w_1 are constrained by the non-interference condition at the maximum opposite deflection angle ($\beta_{lim} = 45°$ for underwater mode) of adjacent rudders. The distance from the fixed frame axis to the rudder edge is $r = 12.5$ mm, with rudder thickness $t = 13$ mm. These satisfy:

$$l_1 \sin(\beta_{lim}) \leq (r - t/2) \tag{13}$$

Thus, $l_1 \leq 8.5$ mm. w_1 and l satisfy:

$$l \sin \beta_{lim} \leq (r + w_1 - t/2) \tag{14}$$

Hence, $w_1 \geq l \sin \beta_{lim} + t/2 - r$. Rudder area S relates to l as:

$$\begin{aligned} S &= (l + l_1)w - w_1(l - l_1)/2 \\ &\geq (l + l_1)w - (l \sin \beta_{lim} + t/2 - r)(l - l_1)/2 \end{aligned} \tag{15}$$

TABLE III
CONSTRAINT CONDITIONS OF THE HAUV

Description	Symbol	Value
Thrust coefficient	C_T	0.138
Mass of the vehicle	m	2545 g
Maximum load	m_{load}	1173 g
Maximum attitude deflection	θ	15° (≈0.2618 rad)
Maximum angular acceleration	α	10 rad/s^2
Maximum propeller speed(full-load)	n_{max}	12,000 rpm
Propeller diameter	D	0.267 m
CoL–CoG offset(full-load)	d_{lg}	0.06 m
CoG–rudder axis distance(full-load)	h	0.078 m
Pitch torque of inertia(full-load)	$I_{\text{pitch,max}}$	0.097621 kg · m^2
Rudder installation space	w	0.115 m

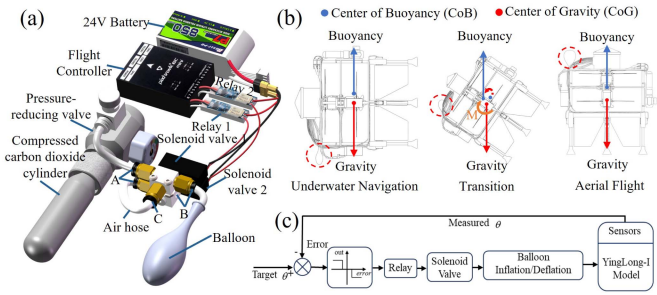

Fig. 5. Attitude switching module design and principle. (a) Module composition diagram. (b) Attitude transition mechanism: Initial neutral-buoyancy balance with CoB above CoG, transition triggered by balloon inflation which generates torque as buoyancy increases and its center shifts, and final vertical stability with CoB realigned above CoG. (c) Closed-loop control diagram of balloon inflation/deflation.

Substituting (15) into (8) and then into (12) yields an inequality with l as the primary variable. Applying maximum-load constraints (Table III) yields minimum dimensions $l = 10$ cm and $S = 0.0091$ m^2. Equation (9) gives a required servo torque of 0.35 N · m (3.57 kg· cm) and a 7 kg· cm servo is selected for safety margin.

D. Attitude Switching Module

To address the conflicting attitude requirements between underwater (horizontal) and aerial (vertical) environments, a gas-driven buoyancy module (Fig. 5(a)) was developed for rapid attitude switching. Inspired by inflatable concepts [19], this module enables faster mode transitions than CoG adjustment methods [13].

Fig. 5(b) illustrates the horizontal-vertical attitude-switching process during balloon inflation. In underwater mode, the vehicle maintains a horizontal attitude with neutral buoyancy, where the center of buoyancy (CoB) is collinear with and above the CoG. Upon inflation, the increasing buoyancy shifts the CoB as depicted in the second subfigure of Fig. 5(b). The resulting offset between CoB and CoG generates a pitching moment, transitioning the vehicle from horizontal to vertical. Inflation ceases when the CoB and CoG realign vertically, stabilizing the vehicle in the upright position.

The inflation volume of the balloon is regulated by a closed-loop control based on the vehicle's attitude, as illustrated in Fig. 5(c). During the transition, the pitch angle is continuously monitored to adjust the gas flow. The controller stops inflation

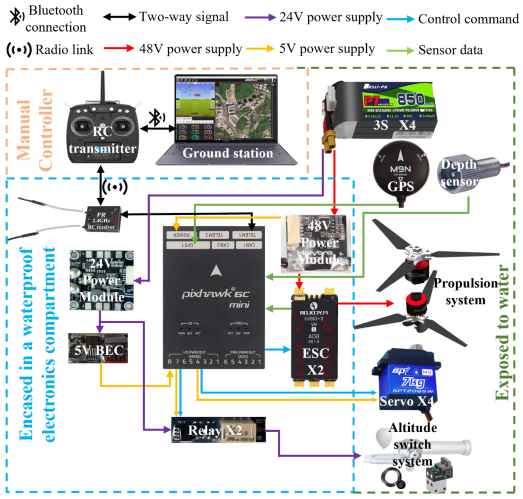

Fig. 6. Schematic diagram of the design, composition and connections of the avionics system.

when the pitch angle reaches the $\pm 5^{\circ}$ threshold from the vertical, and determines further inflation/deflation based on the sign and magnitude of the angular deviation beyond this window.

The current prototype is equipped with an 8 g CO_2 cylinder, enabling 8 horizontal-vertical transitions before replacement to meet most application needs. However, it does not support infinite repeated attitude switching, and its 298 g weight is suboptimal for HAUVs. Future work will focus on enhancing cycle life and reducing module mass.

E. Electronic Equipment

The avionics system's design, composition, and connections are shown in Fig. 6. A Pixhawk 6c mini flight controller serves as the control module, managing the cross-domain movement and integrating sensors/communication interfaces for external devices (e.g., GPS, depth sensor). Power is supplied by four series-connected 3S lithium-ion batteries (outputting 48 V/24 V), monitored by an ammeter. Voltage is regulated via BECs for the flight control system and servos, while ESCs and the relay are directly powered. Communication relies on a 2.4 GHz RC system.

To optimize space and weight distribution, the battery pack is externally mounted after waterproofing. This avoids increasing the volume of the waterproof electronics compartment and helps achieve a suitable CoG.

IV. Proposed Control Strategy

A. PID-Based Motion Control

A dual-closed-loop PID control strategy is adopted for both aerial and underwater modes, leveraging the unified propulsion and attitude control module in Section III. This approach uses a common control algorithm across media, with parameter and sensor adaptations for air/water environments. For aerial control, a Pixhawk 6 C mini flight controller with ArduPilot Copter firmware is used. For underwater operation, a custom mode was

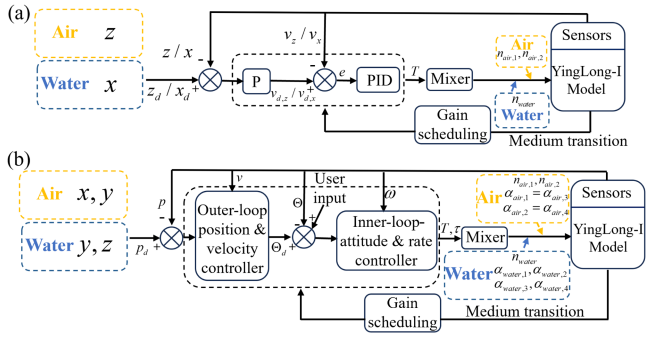

Fig. 7. PID-based control schematic diagram. (a) Decoupled position control. (b) Position and attitude-coupled control.

developed within ArduPilot to reuse its robust PID control code. This strategy enables seamless mode switching, avoids extra control boards/communication overhead, and reduces overall control system complexity.

Fig. 7 depicts the vehicle's control framework. Owing to its underactuated nature in both air and water, the vehicle's motion control exhibits significant coupling. In aerial flight, horizontal X/Y translations are underactuated, requiring indirect control via roll/pitch adjustments. Similarly, underwater navigation lacks direct Y/Z-axis actuation, necessitating yaw/pitch-based attitude control for position/depth management. A cascaded PID controller structure is employed for both position and attitude loops: the inner (velocity) loop enhances dynamic response and disturbance rejection, while the outer (position) loop ensures precise positioning via stable velocity control.

In underwater motion control, position and velocity measurements are critical. Given the high costs of DVL and acoustic positioning systems, our HAUV is not equipped with such devices. We employ a low-cost sensor fusion strategy: integrating acceleration and angular velocity from an IMU, absolute heading from a magnetometer, and absolute depth from a depth sensor to estimate underwater relative displacement (Δx, Δy, Δz) and velocity. The IMU calculates motion and position via double integration but suffers from drift; the magnetometer corrects heading drift and aligns estimates with the Earth coordinate frame; the depth sensor constrains vertical (Z-axis) integration drift. Periodic surfacing enables GPS calibration to reset cumulative errors, balancing basic accuracy against cost constraints.

To avoid gimbal lock when using a single flight control system for both aerial and underwater operations, we use quaternions in control and sensor fusion algorithms for internal attitude calculations—to Euler angles only for external use—to inherently prevent singularities. Pitch angles are constrained to $\pm 15^{\circ}$ (aerial) and $\pm 45^{\circ}$ (underwater) to avoid the $\pm 90^{\circ}$ deadlock zone, with these limits hard-coded in the control logic. To prevent gimbal lock from a 90° pitch shift during mode switching with a shared coordinate system, independent local frames are set for aerial and underwater modes. The flight controller's mounting orientation is reset during transitions to align its system with the HAUV's frame for accurate attitude measurement. This

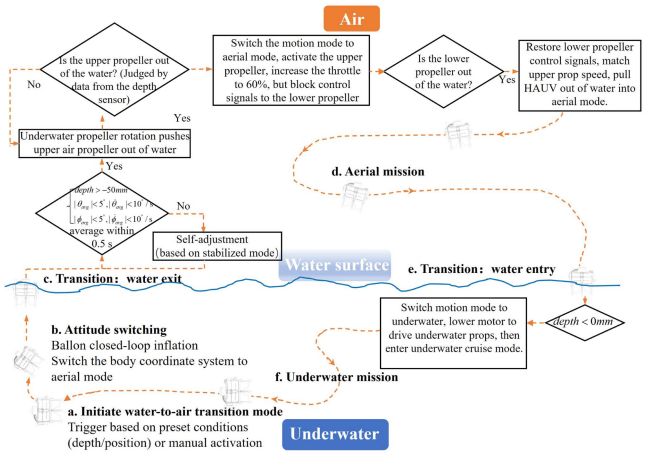

Fig. 8. Cross-domain transition strategy: complete process and switching conditions.

integrated approach robustly mitigates gimbal lock across all operational scenarios.

The PID controller outputs normalized dimensionless forces and torques, distributed to motors/servos via an allocation matrix (termed "mixer" in Fig. 7).

B. Cross-Domain Transition Control

The proposed cross-domain transition strategy targets low-disturbance aquatic environments, framing the process as a mode-transition decision framework rather than an independent motion phase. Activation criteria are defined based on depth thresholds, attitude stability, and angular rate constraints to ensure reliable switching, with thrust activation/deactivation scheduled to avoid hydrodynamic/aerodynamic interference at the medium interface. The complete cross-domain transition strategy is shown in Fig. 8. This static threshold-based approach prioritizes low-complexity switching under calm water conditions, differentiating it from dynamic modeling strategies designed for high-disturbance scenarios.

V. Experimental Validation and Performance Evaluation

A. Aerial Flight Performance Evaluation

Aerial flight performance was evaluated through dedicated indoor flight control teststext and outdoor long-distance experiments. Indoor tests assessed stability and maneuverability, while outdoor experiments measured altitude, speed, distance, and endurance.

The flight log in Fig. 9(a)–(d) records remote control (RC) commands (throttle, pitch, roll) and the controller's tracking performance for pitch/roll angles, alongside voltage, current, and rudder servo angle data. The test includes three phases: hover ($0 - T_1$), horizontal flight ($T_1 - T_2$), and emergency maneuvers (post-T_2). As shown in Fig. 9(b), hover tests demonstrated excellent stability with pitch/roll angles fluctuating $\leq 3°$. During the horizontal flight, pitch angle stability enabled constant-velocity level flight. The controller's precise tracking of RC commands

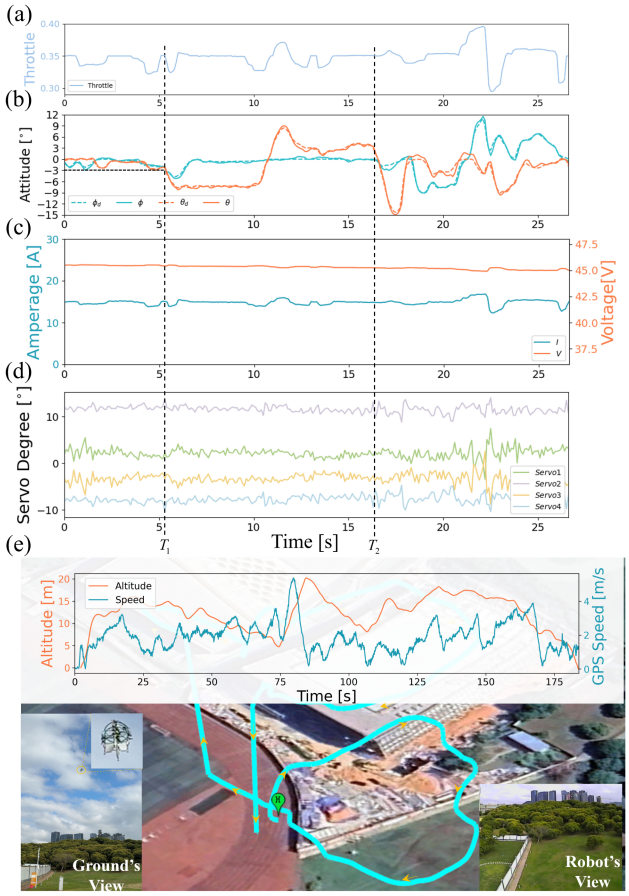

Fig. 9. YingLong-I: Multi-scenario flight validation. (a)-(d) Flight log during dedicated indoor flight control tests. (e) Outdoor flight and experimental data.

during emergency maneuvers validated excellent aerial maneuverability. Additionally, indoor obstacle-hoop navigation experiments were conducted to assess the prototype's suitability for indoor tasks, with experimental procedures detailed in the supplementary video material.

Compared with multi-rotor vehicles [8] showing fluctuating voltage/current, our vehicle exhibits smoother profiles in Fig. 9(c). This is attributed to its rudder-based attitude control system, as evidenced by real-time rudder angle adjustments in Fig. 9(d) with negligible servo power consumption. By contrast, multi-rotor systems relying on motor speed adjustments for attitude exhibit larger voltage/current fluctuations, leading to higher energy consumption and electromagnetic interference. Our design thus offers distinct advantages in energy efficiency and electromagnetic compatibility.

Outdoor testing (Fig. 9(e)) was conducted in level 3 wind ($\approx$ 8 m/s). GPS and flight logs show a maximum speed of 5.4 m/s, average speed of 2.35 m/s, maximum climb rate of 3.6 m/s, and flight altitude of 5–20 m. Endurance estimates based on flight time, power consumption, and battery capacity were 7.5 min with a 2200 mAh battery. Compared with TJ-FlyingFish [18], our design has a larger takeoff weight (2.5 kg vs. 1.63 kg) and longer flight time (7.5 min vs. 6 min) with the same 2200 mAh battery, proving the co-axial configuration's better energy efficiency.

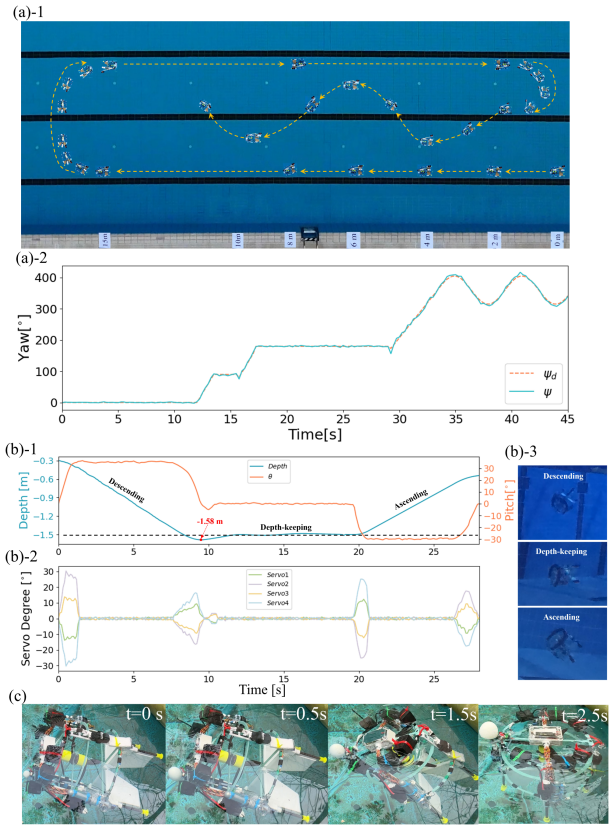

Fig. 10. Underwater experiments. (a-1) Navigation trajectory in water: straight line, turning maneuvers, and S-maneuvers. (a-2) Performance log of heading control. (b-1) Variation of depth and pitch angle (θ) during descending, depth-keeping, and ascending phases. (b-2) Variation of rudder deflection angles during descending, depth-keeping, and ascending phases. (b-3) Different vehicle status. (c) Horizontal-to-vertical attitude-switching sequence.

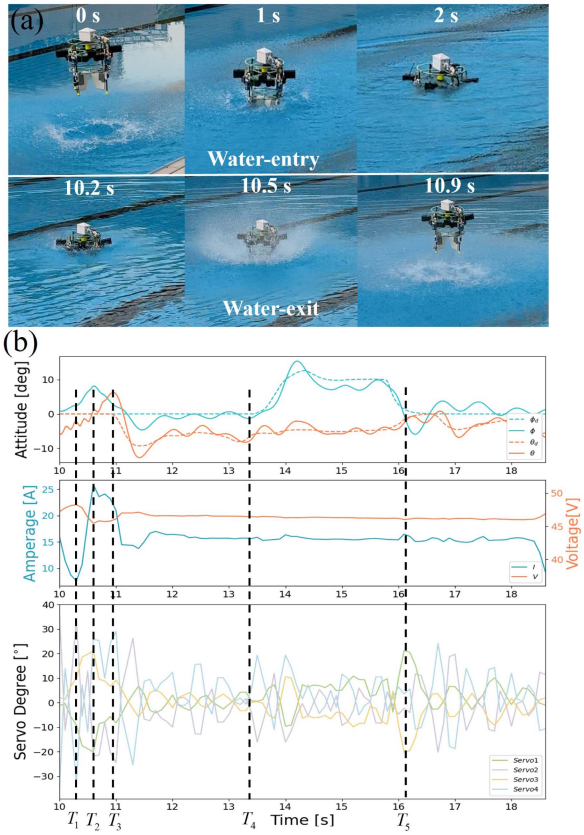

Fig. 11. (a) Sequence diagram of the cross-domain locomotion. (b) Flight logs including attitude, power, and servo degrees.

B. Underwater Maneuverability Assessment

Underwater maneuverability was experimentally validated in an outdoor pool, including straight-line navigation, 90°/180° turns, and S-maneuvers (Fig. 10(a-1)). Straight-line tests showed consistent 1 m/s navigation at 30% throttle, reaching 1.8 m/s at 50%. For 180° rapid turns, the vehicle achieved a 1.1 m minimum turning radius in 4 seconds. Fig. 10(a-2) demonstrated effective heading control: under various preset conditions, the controller maintained heading error within 6°, validating its robustness and tracking performance. The maximum speed outperforms other HAUVs listed in Table I, enabled by the integrated propulsion system with underwater performance comparable to separate systems, combined with a compact co-axial design that reduces drag. Based on flight time, power consumption, and battery capacity calculations, the estimated navigation time at 0.25 m/s is 50 min—outperforming TJ-FlyingFish (40min) and comparable to Longbow-II (57min) and TDAV (55min). This is attributed to high-efficiency integrated propulsion system, the energy-efficient attitude control system, and the neutral buoyancy design.

C. Depth-Keeping Performance Evaluation

During depth control tests with a target depth of 1.5 m, the maximum pitch angle and rudder deflection were limited to 30°. Results (Fig. 10(b)) show that: the rudder rapidly deflected to 30° to achieve a 30° pitch angle within 0–1.4 s, then returned to neutral; the diving pitch angle was maintained from 1.4–7.6 s. As the target depth was approached (7.6–9.6 s), the rudder adjusted to reduce pitch to zero, with a $\leq$ 0.08 m overshoot corrected by fine adjustments before entering depth-keeping (error $\leq$ 0.03 m). After 10s of depth-keeping, surfacing began with rudder adjustments reversing the diving phase pattern. The diving overshoot is only 0.08 m, and the depth-keeping error is 0.03 m, fully validating the depth-keeping control performance of YingLong-I.

D. Cross-Domain Transition Experiments

Fig. 10(c) shows sequence frames of the attitude switch module transitioning from horizontal to vertical posture in 2.5 s. Performed during vehicle motion, the transition achieved vertical posture accuracy within $\pm 5°$, validating the module's rapid, precise, and reliable performance.

Aerial-underwater transition experiments validated the vehicle's cross-domain locomotion. As shown in Fig. 11(a), YingLong-I transitioned to underwater operation via a 0.1 m freefall (1 s duration) to minimize water entry impact. After completing underwater tasks, the vehicle shifted from horizontal to vertical posture in 2.5 s, exited the water within 0.7 s. Over six consecutive trials, it demonstrated consistent rapid entry/exit transitions with 100% success, validating the reliability of its cross-domain mobility. YingLong-I's water-exit time

(3.2 s) outperforms TDAV (60 s) [13], thanks to its inflatable attitude-switching module operating faster than TDAV's CoG adjustment, eliminating propeller deployment, and transition strategy. Its single-phase water-exit time (0.7 s) also surpasses Nezha-B(2 s) [8], as the coaxial dual-rotor configuration avoids lift imbalance issues caused by single-layer propellers cutting through the air-water interface, ensuring stable attitude control.

The partial flight log in Fig. 11(b) details five locomotion stages: At T_1 (10.2 s), the upper propeller exited the water, triggering 60% throttle activation. The resulting current surge overcame gravity, drag, and surface tension. At T_2, the lower propeller rose out of the water, activated to add lift and reduce current. T_2–T_3 corresponds to 10.5–10.9 s in Fig. 11(a). From T_3–T_4, the vehicle transitioned to forward flight, followed by lateral maneuvers in T_4–T_5. Controller attitude tracking was not optimal: flight at near-water altitude (≈ 1 m) caused downwash-induced surface disturbance, slightly impacting tracking. Future work will enhance the controller's disturbance rejection.

E. Load Capacity Experiments

During payload tests, the vehicle achieved stable takeoff with a 1173 g ($\approx$ 1.2 kg) payload(payload-to-weight ratio: 0.46) and showed good maneuverability. Flight data showed a 60% average throttle, 24.4 A current, and 1160 W power consumption. This payload-to-weight ratio outperforms all HAUVs in Table I due to its co-axial design, which enables a larger rotor area for greater load capacity while maintaining a compact structure.

VI. Conclusion

This letter presents YingLong-I, a compact (292$\times$ 292$\times$ 405 mm), 2.5 kg HAUV featuring an integrated coaxial counter-rotating propulsion module and a water-air compatible attitude control system. The coaxial design simplifies structure, reduces volume and weight, and improves multi-medium efficiency compared to other integrated solutions. The rudder-based attitude control module uses identical hardware/strategies in both media, minimizing additional hardware and control complexity. Leveraging a compressed gas-based attitude switch module and dedicated control strategy, YingLong-I achieves rapid cross-domain locomotion: a 2.5 s underwater-to-aerial attitude transition and 0.7 s water exit. Notably, it outperforms multi-rotor HAUVs in payload capacity (1.2 kg, payload-weight ratio 0.46). Field experiments validate its aerial, underwater, and cross-domain capabilities. Future research will focus on enhancing attitude-switching repeatability and reducing module weight. Additionally, optimizing the design and control algorithms will enable reliable cross-domain operations in realistic marine environments.

References

[1] C. Li and S. Guo, "Characteristic evaluation via multi-sensor information fusion strategy for spherical underwater robots," *Inf. Fusion*, vol. 95, pp. 199–214, 2023.

[2] A. Li, S. Guo, and C. Li, "An improved motion strategy with uncertainty perception for the underwater robot based on thrust allocation model," *IEEE Robot. Automat. Lett.*, vol. 10, no. 1, pp. 64–71, Jan. 2025.

[3] S. Guo, T. Fukuda, and K. Asaka, "A new type of fish-like underwater microrobot," *IEEE/ASME Trans. Mechatron.*, vol. 8, no. 1, pp. 136–141, Mar. 2003.

[4] F. M. Rockenbauer et al., "Dipper: A dynamically transitioning aerial-aquatic unmanned vehicle," *Robot., Sci. Syst. XVII*, vol. 2021, pp. 12–16, 2021.

[5] R. Puppala, N. Sivadasan, A. Vyas, A. Molawade, T. Ranganathan, and A. Thondiyath, "Design, estimation of model parameters, and dynamical study of a hybrid aerial-underwater robot: Acutus," in *Proc. Int. Conf. Informat. Control, Automat. Robot.*, 2019, pp. 423–430.

[6] Y. Jin, Z. Zeng, and L. Lian, "Nezha-SeaDart: A tail-sitting fixed-wing vertical takeoff and landing hybrid aerial underwater vehicle," *J. Field Robot.*, vol. 61, no. 1, pp. 137–152, 2024.

[7] X. Sun, J. Cao, Y. Li, and B. Wang, "Design and field test of a foldable wing unmanned aerial–underwater vehicle," *J. Field Robot.*, vol. 41, pp. 347–373, 2023.

[8] Y. Bi, Z. Xu, Y. Shen, Z. Zeng, and L. Lian, "Design and implementation of a bone-shaped hybrid aerial underwater vehicle," *IEEE Robot. Automat. Lett.*, vol. 9, no. 8, pp. 7318–7325, Aug. 2024.

[9] Y. Bai, Y. Jin, C. Liu, Z. Zeng, and L. Lian, "Nezha-F: Design and analysis of a foldable and self-deployable HAUV," *IEEE Robot. Automat. Lett.*, vol. 8, no. 4, pp. 2309–2316, Apr. 2023.

[10] M. M. Maia, D. A. Mercado, and F. J. Diez, "Design and implementation of multirotor aerial-underwater vehicles with experimental results," in *Proc. IEEE/RSJ Int. Conf. Intell. Robots Syst.*, 2017, pp. 961–966.

[11] X. Yuan, W. Bian, Q. Zhao, and G. Zhao, "Numerical investigation of aerodynamic interactions for the coaxial rotor system in low-speed forward flight," *Aerosp. Sci. Technol.*, vol. 149, 2024, Art. no. 109148.

[12] H. Zhang, Z. Zeng, C. Yu, J. Zhining, B. J. Han, and L. Lian, "Predictive and sliding mode cascade control for cross-domain locomotion of a coaxial aerial underwater vehicle with disturbances," *Appl. Ocean Res.*, vol. 100, 2020, Art. no. 102183.

[13] Y. Gao, H. Zhang, G. J. Li, M. Zhou, H. Yin, and T. A. Gulliver, "Analysis of trans-domain motion process of bullet-shaped trans-domain amphibious vehicle," *J. Field Robot.*, vol. 41, pp. 68–92, 2023.

[14] C. Wang, Q. Hui, and F. Zhang, "Design of water-air cross-domain multi-mode coaxial UAV," *Acta Aeronautica et Astronautica Sinica*, vol. 44, no. 21, 2023, Art. no. 529047.

[15] H. Alzu'bi, O. Akinsanya, N. Kaja, I. Mansour, and O. Rawashdeh, "Evaluation of an aerial quadcopter power-plant for underwater operation," in *Proc. 10th Int. Symp. Mechatron. Appl.*, 2015, pp. 1–4.

[16] G. Yao et al., "Review of hybrid aquatic-aerial vehicle (HAAV): Classifications, current status, applications, challenges and technology perspectives," *Prog. Aerosp. Sci.*, vol. 139, 2023, Art. no. 100902.

[17] Y. H. Tan, R. Siddall, and M. Kovac, "Efficient aerial–Aquatic locomotion with a single propulsion system," *IEEE Robot. Automat. Lett.*, vol. 2, no. 3, pp. 1304–1311, Jul. 2017.

[18] X. Liu et al., "TJ-FlyingFish: Design and implementation of an aerial-aquatic quadrotor with tiltable propulsion units," in *Proc. IEEE Int. Conf. Robot. Automat.*, 2023, pp. 7324–7330.

[19] D. Lu et al., "Design, fabrication, and characterization of a multi-modal hybrid aerial underwater vehicle," *Ocean Eng.*, vol. 219, 2021, Art. no. 108324.